Renner−Teller Effect in $C_2H_2^+(X^2\Pi_u)$ Studied by Rotationally Resolved Zero Kinetic Energy Photoelectron Spectroscopy

Jie Yang and Yuxiang Mo*

Department of Physics and Key Laboratory for Atomic and Molecular Nanosciences, Tsinghua University, Beijing 100084, China

Received: May 25, 2006; In Final Form: July 24, 2006

The Renner−Teller effect in $C_2H_2^+(X^2\Pi_u)$ has been studied by using zero kinetic energy (ZEKE) photoelectron spectroscopy and coherent extreme ultraviolet (XUV) radiation. The rotationally resolved vibronic spectra have been recorded for energies up to 2000 cm^{-1} above the ground vibrational state. The C≡C symmetric stretching (υ_2), the CCH trans bending (υ_4), and the CCH cis bending (υ_5) vibrational excitations have been observed. The assigned vibronic bands are $4_1^1(\kappa^2\Sigma_u^+)$(hot band), $4_0^1(\mu/\kappa^2\Sigma_u^{-/+})$, $5_0^1(\mu/\kappa^2\Sigma_g^{+/-})$, and $4_0^2(\mu^2\Pi_u)$, $4_0^2(\kappa^2\Pi_u)$, $4_0^15_0^1(\mu^2\Pi_g)$, $0_0^0(X^2\Pi_u)$, and $2_0^1(X^2\Pi_u)$. The Renner−Teller parameters, the harmonic frequencies, the spin−orbit coupling constants, and the rotational constants for the corresponding vibronic bands have been determined by fitting the spectra with energy eigenvalues from the Hamiltonian that considers simultaneously Renner−Teller coupling, vibrational energies, rotational energies, and spin−orbit coupling interaction.

I. Introduction

The coupling of the degenerate electronic state with the bending vibrational state in linear molecules is called the Renner−Teller effect. It is one of the clear examples of the breakdown of the Born−Oppenheimer approximation. There is a lot of research about the Renner−Teller effect in various linear triatomic molecules.[1,2] For linear tetratomic molecules, experimental research has been done mainly for the following molecules, $C_2H_2/C_2H_2^+$, HCCS, and HCCSe.[3−9] In comparison with triatomic molecules, the linear tetraatomic molecules have two bending modes, the trans and cis bending vibrations, and both of them are Renner−Teller active. This makes the rovibronic structures of the tetraatomic molecules much more complicated than those in the triatomic molecules.

Among several linear tetraatomic molecules with Renner−Teller effect, $C_2H_2^+(X^2\Pi_u)$ is the simplest one and has been studied in the most detail.[6−9] In the high-resolution photoelectron spectroscopic (PES) study, the energy splittings due to the coupling of degenerate electronic state with trans (υ_4) and cis (υ_5) bending vibrations in $C_2H_2^+$ have been suggested.[6] However, because of the limited resolution (∼20 cm^{-1}) of PES spectra, no quantitative information was obtained. Using two color excitation and zero-kinetic energy (ZEKE) photoelectron spectroscopic methods, Pratt et al.[7] had done partially rotationally resolved studies for the trans bending vibration up to $\upsilon_4 = 3$. Because an intermediate state ($\tilde{A}^1A_u$) with trans bending geometry was used in their excitation scheme, cis bending vibration was not observed. Using the XUV laser and ZEKE method, Rupper and Merkt obtained the rotationally resolved ground vibrational band of $C_2H_2^+$ and accurate ionization potential was obtained.[9] Very recently, cis bending vibrational excitation ($\upsilon_5 = 1$) has been observed using IR absorption and laser-induced reaction method.[8] In that work, a total of seven vibronic bands are used to fit a heavily overlapped spectrum to obtain vibrational frequency and also the Renner−Teller parameter for cis bending vibration.

In this paper, we report fully rotationally resolved studies on $C_2H_2^+(X^2\Pi_u)$ using ZEKE photoelectron spectroscopic and the XUV laser method. Vibronic bands up to 2000 cm^{-1} above the ground vibrational state or 11.39−11.65 eV above the neutral molecule have been observed, which includes both cis and trans bending vibrational modes.

For linear triatomic molecules, theoretical methods have been developed to calculate the rovibronic energy levels using Renner−Teller parameters, spin−orbit coupling constants and rotational constants of the molecule.[2,10,11] Because of the vibronic coupling, different vibrational states are coupled via the Renner−Teller effect.[10] When the harmonic wave function is used as the basis function to calculate the Hamiltonian matrix elements, in principle, an infinite number of vibrational quantum numbers are needed to obtain exact energy eigenvalues.[10] Presently, the off-diagonal Renner−Teller terms among different vibrational states are usually replaced by diagonal energy corrections to the vibration energies by using perturbation theory.[2,10] This treatment is valid only for weak Renner−Teller coupling.

For handling the tetra-atomic molecules with spin−orbit interaction, Peric and co-workers have found a series of formulas derived from the perturbation theory to calculate the vibronic energy levels[12−14] Recently, He and Clouthier have developed very complete treatments which consider not only the Renner−Teller effect but also the anharmonic couplings among different vibrational modes.[4,5] However, rotational excitations have not been considered in these two treatments. The rovibronic energy levels of tetraatomic molecules could be calculated straightforwardly by combining Peric and his co-worker's formula with Hougen's procedure of taking the rotational energy into the consideration.[11] The analytic formula for this would become very complicated and their accuracies are difficult to predict because of the perturbation theory used in the treatments. With the present computational power, in fact, it is much more accurate and convenient to set up the whole Hamiltonian which

* To whom correspondence should be addressed. E-mail: ymo@mail.tsinghua.edu.cn.

10.1021/jp063209t CCC: $33.50
Published on Web 09/06/2006

considers simultaneously the matrix elements of Renner−Teller interaction, vibrational energies, rotational energies, and spin−orbit interactions and to solve this Hamiltonian directly to obtain the rovibronic energy levels. In this paper, we report the fitting of our rotationally resolved spectra of $C_2H_2^+(X^2\Pi_u)$ by using such a method. The vibrational frequencies, spin−orbit coupling constants and Renner−Teller parameters have been determined by fitting the spectra using the nonlinear least-squares method.

II. Experimental Method

The XUV photoelectron and photoion spectrometer used in this work has been described in detail.[15] Briefly, coherent XUV radiation was generated by using the resonance enhanced four-wave sum mixing in a pulsed Xe jet. A Nd:YAG (20 Hz) pumped two dye laser system was used to prepare the fundamental frequency laser beams. One beam produced by doubling the dye laser frequency was fixed to match the two-photon resonance ($2\omega_1$) frequency of the Xe $5p^5(^2P_{3/2})6p[1/2]_0 \leftarrow (5p^6)^1S_0$ transition at 80 119.0 cm^{-1}. The other beam (ω_2) was tuned from 720 to 850 nm by using different laser dyes. The two fundamental beams were merged by a dichroic mirror and focused by an achromatic lens (250 mm) into a pulsed Xe jet. The apparatus consists of four vacuum chambers: (a) the frequency mixing chamber, which houses a pulse Xe jet (ϕ 1 mm); (b) the monochromator chamber, which is equipped a gold coated toroidal grating; (c) the beam source chamber, which houses a pulse valve (ϕ 0.7 mm) to produce a pulse molecular beam (the beam enters into the ionization chamber through a skimmer (ϕ 1 mm)); (d) the ionization chamber, which houses an ion and an electron time-of-flight (TOF) spectrometers together with a set of dual microchannel plate (MCP) detectors each for charge particle, respectively (a separate MCP detector is installed in this chamber to monitor the XUV intensity).

The electron signals from the pulsed field ionization and the XUV radiation signals were fed into two identical boxcars (SR 245, Stanford Research Systems) before further processing by a personal computer. The pulses used to synchronize the two pulse valves and the Nd:YAG laser were provided by a digital delay generator (DG 535, Stanford Research Systems). The pulse voltages for field ionization were provided by another DG 535 with high voltage option.

The C_2H_2 gas sample was premixed with He (He 90%, C_2H_2 10%) or with Ne (He 95%, C_2H_2 5%) and the stagnation pressure used was about 1000 Torr at the room temperature. In the experiments, the pressures for beam source and ionization chamber were around 2×10^{-3} and 1×10^{-5} Pa, respectively. The temperature of the supersonic cooled C_2H_2 beam is less than 10 K for Ne carrier gas or around 50 K for He carrier gas. The frequencies of the tuning dye laser were calibrated by using the He/Ne and He/Ar optogalvanic lamp. The uncertainties of photon energy after the calibration were less than 0.5 cm^{-1}.

A discriminative pulsed electric field of 0.1 V/cm was used to remove the prompt electrons with a delay of 0.3 μS relative to the XUV laser pulse. Great care has also been taken to avoid the autoionization signals in the ZEKE spectra. The pulsed electric fields used to ionize the Rydberg molecules were about ±0.5 V/cm with delays about 2−3 μS relative to the XUV laser pulse. The spectral resolution thus obtained was about 0.8 cm^{-1} (full width at half-height). The uncertainties of the relative rotational line positions were about 0.2 cm^{-1}. After taking account of the Stark effect, the uncertainties of the absolute line positions were about 1 cm^{-1}.

III. Theoretical Background

A. Rovibronic Energy Level Calculation Considering Simultaneously Renner−Teller Interaction, Vibrational Energies, Rotational Energies, Spin−Orbit Interaction. The ground electronic state of $C_2H_2^+(X^2\Pi_u)$ has $D_{\infty h}$ symmetry. It has five vibrational modes which are designed as $(v_1v_2v_3v_4v_5)^+$, where v_1 and v_3 represent the symmetric and antisymmetric C≡C stretching vibrations, v_2 represents the C−C stretching vibration, v_4 and v_5 represent the degenerate CCH trans and cis bending vibrations, respectively.

For linear triatomic molecule, the effective Hamiltonian including the Renner−Teller interaction, rotational energies, and spin−orbit interaction in a $^{2s+1}\Pi$ state has been discussed in detail.[2,16,17] For tetratomic molecules, the two bending modes v_4 and v_5 are both Renner−Teller active. The effective Hamiltonian should include the Renner−Teller interaction of the two vibrational modes.

The Hamiltonian of the molecule is expressed as

$$H = T_{vib} + H_{so} + H_{rot} + H_{RT} \quad (1)$$

where T_{vib}, H_{so}, H_{rot}, and H_{RT} are terms due to the vibrational motion, spin−orbit coupling, molecular rotation and vibronic coupling (Renner−Teller effect). They are as follows,[17]

$$T_{vib} = \omega_4(v_4+1) + \omega_5(v_5+1) \quad (2)$$

$$H_{rot} = B^+(m,n)R^2 \quad (3)$$

$$H_{so} = A_{SO}L_zS_z \quad (4)$$

$$H_{RT} = \frac{1}{2}\epsilon_4\omega_4(q_{4+}{}^2\exp(-2i\theta_4) + q_{4-}{}^2\exp(2i\theta_4)) + \frac{1}{2}\epsilon_5\omega_5(q_{5+}{}^2\exp(-2i\theta_5) + q_{5-}{}^2\exp(2i\theta_5)) \quad (5)$$

where ω_4, ω_5 and ϵ_4, ϵ_5 are the harmonic frequencies and Renner−Teller parameters, for v_4 and v_5 vibrational modes, respectively. $B^+(m,n)$ is the rotational constant for vibrational quantum numbers of $v_4 = m$ and $v_5 = n$. The A_{SO} is the spin−orbit coupling constant. $q_{4\pm}$, $q_{5\pm}$ and θ_4, θ_5 are the dimensionless vibrational ladder operators and the electronic azimuthal angles for v_4 and v_5 vibrational modes, respectively.

The nuclear rotational angular momentum R is expressed by

$$R = J - G - L - S \quad (6)$$

where J is total angular momentum, G is the vibrational angular momentum, L is the electronic angular momentum and S is the total electronic spin. We have[11]

$$R^2 = (J^2 - J_z^2 + S^2 - S_z^2 - G_z^2) - (J_+S_- + J_-S_+) \quad (7)$$

We use the basis function of Hund' case (a), $|\Lambda,\Sigma,J,v_4,l_4,v_5,l_5;P,K\rangle$, where Λ and Σ are the projections of electronic orbital angular momentum and spin angular momentum on the molecular axis, respectively. The K and P are the projections of total angular momentum excluding electron spin and the total angular momentum on the molecular axis, respectively, i.e.

$$K = l_4 + l_5 + \Lambda \qquad K \geq 0 \quad (8)$$

$$P = l_4 + l_5 + \Lambda + \Sigma = K + \Sigma \qquad \Sigma = \pm 1/2 \quad (9)$$

Figure 1 shows the relationship among these parameters.

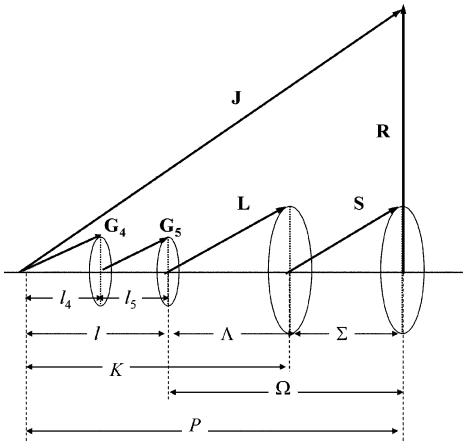

Figure 1. Schematic diagram about the quantum numbers used in the Hund's case (a) basis $|\Lambda,\Sigma,J,v_4,l_4,v_5,l_5;P,K\rangle$.

When there is Renner−Teller effect, the good quantum numbers are J and K in the basis function $|\Lambda,\Sigma,J,v_4,l_4,v_5,l_5;P,K\rangle$. Because of the $J_+S_- + J_-S_+$ term in eq 7, states with different P are mixed. Using the perturbation method, we can set up a Hamiltonian that considers simultaneously the Renner−Teller effect, vibrational energies, rotational energies, and spin−orbit interactions. The matrix elements which are diagonal in quantum numbers P, K,Λ,Σ, v_4 and v_5 are written as[16,17]

$$\langle\Lambda,\Sigma,v_4,l_4',v_5,l_5';J,P,K|H_{vib}+H_{rot}+H_{SO}|\Lambda,\Sigma,v_4,l_4,v_5,l_5;J,P,K\rangle = \{\omega_4(v_4+1)+\omega_5(v_5+1)+B^+(m,n)[J(J+1)-P^2+0.5-(K-\Lambda)^2]+A_{SO}\Lambda\Sigma\}\delta_{l_4+l_5,l_4'+l_5'} \quad (10)$$

There are also off-diagonal matrix elements with respect to P [16,17]

$$\langle\Lambda,\Sigma',v_4,l_4,v_5,l_5;J,P',K|H_{rot}|\Lambda,\Sigma,v_4,l_4,v_5,l_5;J,P,K\rangle = -B^+(m,n)[J(J+1)-P(P\pm1)]^{1/2}\delta_{P',P\pm1} \quad (11)$$

The Renner−Teller interaction is[16,17]

$$\begin{aligned}\langle-\Lambda,\Sigma,v_4',l_4',v_5',l_5';P',K|H_{RT}|\Lambda,\Sigma,v_4,l_4,v_5,l_5;P,K\rangle = {}& \frac{1}{4}\omega_4\epsilon_4\{[(v_4+\Lambda l_4+4)(v_4+\Lambda l_4+2)]^{1/2}\delta_{v_4',v_4+2}\delta_{v_5,v_5'}\delta_{l_5,l_5'}+\\ & 2[(v_4+\Lambda l_4+2)(v_4-\Lambda l_4)]^{1/2}\delta_{v_4',v_4}\delta_{v_5,v_5'}\delta_{l_5,l_5'}+\\ & [(v_4-\Lambda l_4)(v_4-\Lambda l_4-2)]^{1/2}\delta_{v_4',v_4-2}\delta_{v_5,v_5'}\delta_{l_5,l_5'}\}+\\ & \frac{1}{4}\omega_5\epsilon_5\{[(v_5+\Lambda l_5+4)(v_5+\Lambda l_5+2)]^{1/2}\delta_{v_5',v_5+2}\delta_{v_4,v_4'}\delta_{l_4,l_4'}+\\ & 2[(v_5+\Lambda l_5+2)(v_5-\Lambda l_5)]^{1/2}\delta_{v_5',v_5}\delta_{v_4,v_4'}\delta_{l_4,l_4'}+\\ & [(v_5-\Lambda l_5)(v_5-\Lambda l_5-2)]^{1/2}\delta_{v_5',v_5-2}\delta_{v_4,v_4'}\delta_{l_4,l_4'}\} \quad (12)\end{aligned}$$

All other matrix elements not listed in eqs 10−12 are zero.

Using eqs 10−12, we can set up a Hamiltonian for a particular J and K. By assuming constants ω_4, ω_5, ϵ_4, ϵ_5, A_{so} and $B^+(m,n)$, we can obtain energy levels for J and K. In the calculations, we have to truncate the basis set $|\Lambda,\Sigma,J,v_4,l_4,v_5,l_5;P,K\rangle$ to certain maximum numbers of v_4 and v_5, which make the energy levels be converged. Typical values are $v_4 = 7$ and $v_5 = 8$. We used the nonlinear least-squares fitting method to obtain the spectroscopic constants. A satisfactory assignment of spectra should provide the standard deviation of the rotational line positions smaller than the relative experimental uncertainties (±0.2 cm^{-1}).

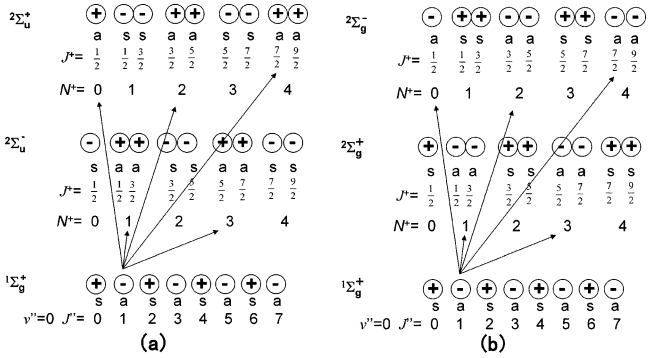

Figure 2. (a) Symmetric properties of $C_2H_2(X^1\Sigma_g^+)$ and the ionic rotational states $^2\Sigma_u^-$ and $^2\Sigma_u^+$. (b) Symmetric properties of $C_2H_2(X^1\Sigma_g^+)$ and the ionic rotational states $^2\Sigma_g^-$, and $^2\Sigma_g^+$. "⊕" ("⊖") indicates that the symmetry of the total wave function is positive (negative). *a* and *s* represent the symmetry of nuclear spin state. N^+ and J^+ represent the nuclear rotation and total rotational angular momentum of the ion, respectively. J'' represents the total angular momentum of the neutral. The arrows show the allowed transitions.

B. Photoionization Selection Rules. In the photoelectron spectroscopy, the Franck−Condon (FC) principle is usually quite good in describing the vibrational band intensities.[15,18,19] The transition intensity from the symmetry ground vibrational state to the degenerate vibrational state with nonzero vibration angular momentum should be zero according to the FC principle. However, if there is strong vibronic interaction, the FC principle cannot be applied simply and the transition to degenerate vibrational state with nonzero angular momentum may be possible. For C_2H_2, the electronic configuration is $(1s\sigma_g)^2(1s\sigma_u)^2$-$(2s\sigma_g)^2(3\sigma_g)^2(2s\sigma_u)^2(1\pi_u)^4$, the ionization will take away the electron in $1\pi_u$. The $1\pi_u$ electron may have orbital angular momentum with $l = 1, 3$. The excitations to vibrational excited states of the ion with $K = 0(\Sigma)$, $1(\Pi)$, $2(\Delta)$, and $3(\Phi)$ are possible,[7] although the calculation of the relative intensities requires a lot of theoretical works.

For C_2H_2, because of the $D_{\infty h}$ symmetry, the two H atom form total nuclear spin states with either symmetry (s) or antisymmetry (a) properties. In photoionization, the symmetry of the spin state should not be changed or the allowed transition is from a to a or from s to s.[7] For states with $K \neq 0$, there are always degenerate rotational energy levels with s and a symmetry. This selection rule does not change the appearance of the spectra. However, this is not true for transition to $K = 0$ or Σ state. Figure 2 shows the selection rules for the rotational transition from the ground vibrational state $C_2H_2(X^1\Sigma_g^+)$ to $K = 0$ state, $^2\Sigma_u^-$ and $^2\Sigma_u^+$, $^2\Sigma_g^-$ and $^2\Sigma_g^+$ of $C_2H_2^+$.

IV. Results and Discussion

A. Overview of the ZEKE Spectra. The survey ZEKE spectrum of C_2H_2 and its assignment is shown in Figure 3. The expanded figures can be found in Figures 6−12. The intensities for different vibronic bands differ so much that they are out of the dynamic ranges of our apparatus under the normal experimental conditions. Thus, the intensities of the spectra shown in Figure 3 have not been normalized. The strongest signals are from the first vibrational band and the C≡C stretching vibrational band. Only very weak bending excitation signals were observed, just as shown by the reported PES spectra.[6] It is due to the fact that the equilibrium geometric structures for the ground electronic states of C_2H_2 and $C_2H_2^+$ are both linear and the C≡C bond lengths have some differences. There were no signals observed in the blank region of the spectra. The assignment of vibronic band is labeled by $V_n^m(^{2s+1}K_{P,g/u})$,

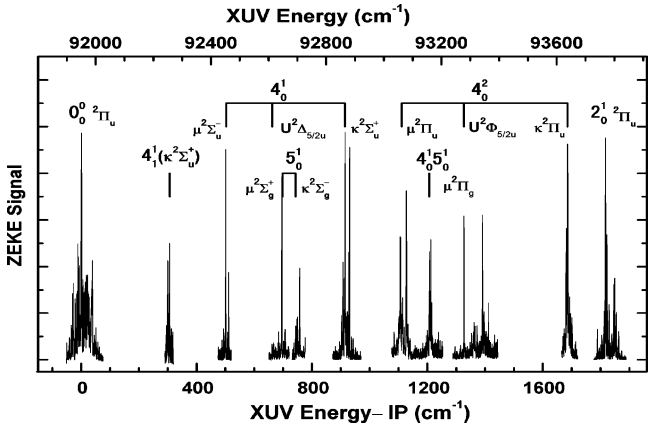

Figure 3. Survey ZEKE spectrum of C_2H_2 and the assignments. On the *x*-axis at the top are the XUV photon energies, and on the *x*-axis at the bottom are XUV photon energies relative to the ionization potential (IP) of C_2H_2. The relative intensities among different vibronic bands have not been normalized. The 4_0^n, 5_0^n, and $4_0^1 5_0^1$ vibronic bands represent the transition from ground vibrational state of C_2H_2 to the *n*'th vibrational state of CCH trans bending, CCH cis bending and combination excitation of trans and cis bending vibrations, respectively.

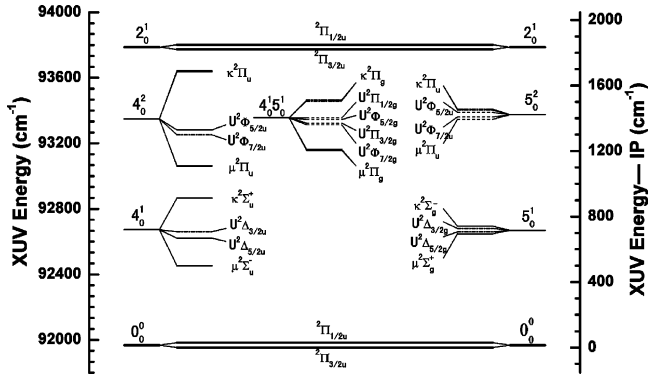

Figure 4. Vibronic energy levels of $C_2H_2^+(X^2\Pi_u)$ calculated by spectroscopic constants determined in this work (see Table 4). The *y*-axis in the left and right represent the photon energy relative to the ground state of C_2H_2 and $C_2H_2^+(X^2\Pi_u)$, respectively. The solid line, dash line, and the dash−dotted lines represent the vibronic bands observed experimentally, vibronic bands which are difficult to be assigned in the ZEKE spectra and vibronic bands not observed experimentally.

where V represents the vibrational mode and *n* and *m* represent the vibrational quantum numbers for neutral and ion, respectively. The coupling of the vibrational angular momentum with the electronic angular momentum is labeled as ${}^{2s+1}K_{P,g/u}$, where *K* and *P* are defined in eqs 8 and 9, respectively. For states with same *K*, we use μ, U, and κ before *K* to represent lower, middle, and higher energy levels, respectively. The g(u) represents the symmetry of electronic and vibrational wave function with respect to the nuclear exchange.

The assigned vibronic bands are $4_1^1(\kappa^2\Sigma_u^+)$ (hot band). $4_0^1(\mu/\kappa^2\Sigma_u^{-/+})$, $5_0^1(\mu/\kappa^2\Sigma_g^{+/-})$, $4_0^2(\mu^2\Pi_u)$, $4_0^2(\kappa^2\Pi_u)$, $4_0^1 5_0^1(\mu^2\Pi_g)$, $0_0^0(X^2\Pi_u)$, and $2_0^1(X^2\Pi_u)$. Other two vibronic bands, $4_0^1(U^2\Delta_{5/2u})$ and $4_0^2(U^2\Phi_{5/2u})$, have been also observed, however, with some uncertainty in the rotational line assignments. Using the spectroscopic constants obtained (see section IVG for details), we have calculated the lowest energy levels of all vibronic bands for energies about 2000 cm^{-1} above the ground vibrational state of $C_2H_2^+(X^2\Pi_u)$, as shown in Figure 4. This figure presents a clear view of the vibronic energy levels due to Renner−Teller effect in $C_2H_2^+(X^2\Pi_u)$.

B. Fitting and Phenomenological Simulation of the Rotationally Resolved ZEKE Spectra. The assignments of a spectrum consist of two aspects: (1) the rotational line positions and (2) the rotational line intensities. The rotational energies can be obtained by assuming spectroscopic constants ω_4, ω_5, ϵ_4, ϵ_5, A_{SO}, $B^+(m,n)$ and solving the Hamiltonian matrix equation using eqs 10−12. The spectroscopic constants are obtained by nonlinear least-squares fitting to the assigned line positions. If the standard deviation between the assigned line positions and the calculated ones is larger than the experimental uncertainty (± 0.2 cm^{-1}), a new assignment has to be tested. In another aspect, the calculation of rotational line strengths is very helpful in the assignment. However, presently, there is no routine method to calculate the rotational line strengths for ZEKE spectroscopy. To overcome this, some phenomenological simulation methods have been developed that are aimed only to extract the spectroscopic constants from experimental data.[15,20] To obtain correct assignments of our rotationally resolved spectra, we made the following assumptions, (1) the rotational line strengths depend only on $\Delta J = |J^+ - J''|$, the relative intensities are varied to obtain the best fitting. (2) The relative ratio between the spin−orbit components $^2\Pi_{3/2}$ and $^2\Pi_{1/2}$ is assumed to be 3:1 (it is found that this value provides better simulation than the value of 2:1). Except these two phenomenological assumptions, the rotational population of the C_2H_2 is determined by the temperature of our molecular beam (50 K for 0_0^0 vibronic band and 6 K for all other vibronic bands) and also the nuclear spin statistics (1:3 for *J* even vs *J* odd). The resolution of our ZEKE spectra (0.8 cm^{-1}) was also taken into consideration in the simulation. Figure 5 shows the comparison of phenomenological simulation and the experimental data. The simulations reproduce the experimental data quite satisfactory except the band $5_0^2(\kappa^2\Sigma_g^-)$ for which the signal intensity cannot be normalized properly because of the very low efficiency of four-wave mixing to produce XUV light. The good simulation of the spectra supports the assignments of the rotational lines which is the main purposes of the simulation.

C. 0_0^0 Transition and C≡C Stretching Vibration 2_0^1. The 0_0^0 vibrational band of $C_2H_2^+(X^2\Pi_u) \leftarrow C_2H_2(X^1\Sigma_g^+)$ in ZEKE spectra has been reported by Rupper and Merkt.[9] In their experiment, the temperature of molecular beam was about 6 K. Panel a of Figure 6 shows the experimental data at rotational temperature of 50 K measured in our lab and the corresponding assignments. Rotational transitions from as high as $J'' = 7$ to other ionic states have been observed.

Panel b of Figure 6 shows the 2_0^1 vibronic band. It is the symmetric C≡C stretching vibration. The rotational temperature of the molecular beam was 6 K in this case. It is seen that most of the transitions are from $J'' = 1$ and 3 due to the nuclear spin statistics.

For 0_0^0 and 2_0^1 vibronic bands, there is no Renner−Teller effect. The rotational line positions can be described simply by the following formula,[21]

$$E(J^+,J'') = T_v + B_v^+\left[\left(J^+ + \frac{1}{2}\right)^2 - 1\right] \pm \frac{1}{2}\sqrt{4B_v^{+2}\left[\left(J^+ + \frac{1}{2}\right)^2 - 1\right] + (A_v - 2B_v^+)^2} - B_0 J''(J''+1) \quad (13)$$

where T_v is the vibronic band origin. B_v^+, A_v, and B_0 are the rotational constant, spin−orbit coupling constant for the ion, and the rotational constant for the neutral,[27] respectively. J^+ and J'' are the total rotational angular momentum for the ion

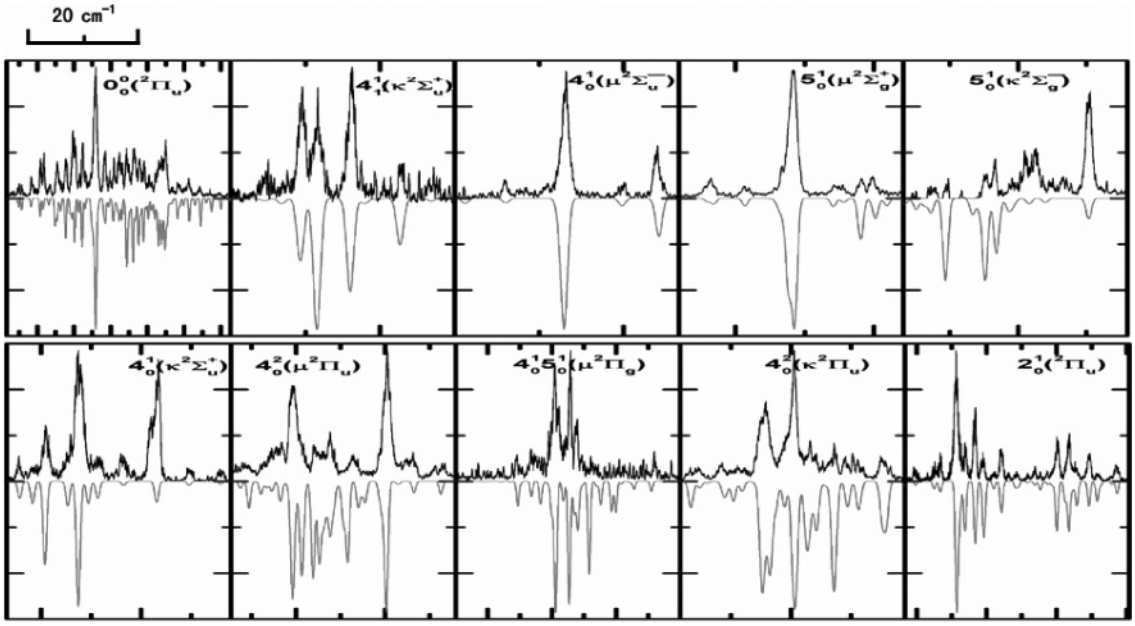

Figure 5. Fitting and phenomenological simulation of the vibronic bands of the ZEKE spectra of C_2H_2. The scale for the *x*-axis is that the photon energy for a major tick is 20 cm^{-1}. The upper parts of the figure are data observed experimentally (expanded ones can be found in Figures 6−11), the lower parts are from the phenomenological simulation in which the rotational distribution of the molecule, the nuclear spin statistics and an assumed rotational line strengths are taken into consideration.

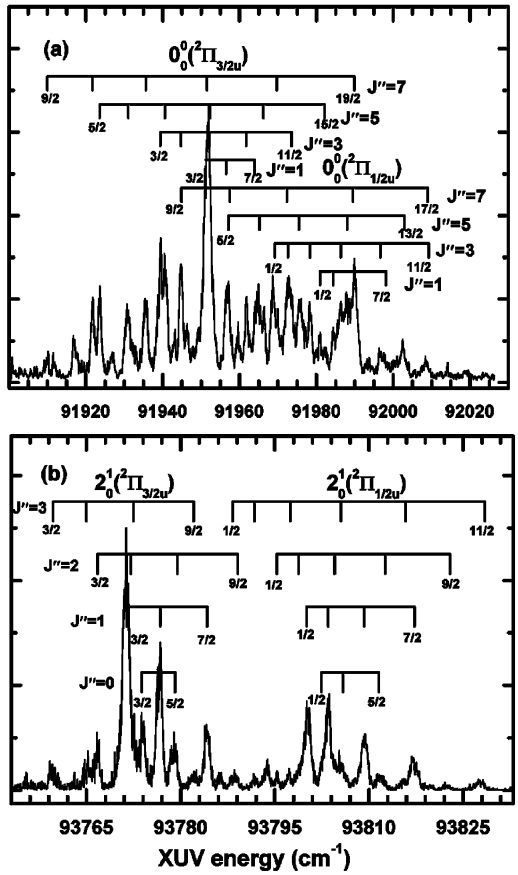

Figure 6. ZEKE spectra and assignments for (a) $C_2H_2^+(X^2\Pi_u) \leftarrow C_2H_2(X^1\Sigma_g^+)$ and (b) $C_2H_2^+(X^2\Pi_u, v_2^+=1) \leftarrow C_2H_2(X^1\Sigma_g^+)$.

and neutral, respectively. Using the nonlinear least-squares fitting method, we determined the spectroscopic constants for 0_0^0 and 2_0^1 vibronic bands. The results are shown in Table 1. Table 2 lists spectral lines used in the fitting along with lines from other vibronic bands. From the fitting, we could also obtain

TABLE 1: Spectroscopic Constants Obtained by Nonlinear Least Square Fitting of 0_0^0 and 2_0^1 Vibronic Bands Using Eq 13[a]

	T_v	B_v^+	A_v
$v^+ = 0$	91966.8(5)	1.104(6)	−30.77(30)
$v_2^+ = 1$	93784.3(5)	1.105(6)	−29.77(12)

[a] All units are in cm^{-1}. The numbers in parentheses are the uncertainties in the last significant figures quoted.

the ionization potential (IP) of C_2H_2 and fundamental symmetric C≡C stretching frequency ω_2 of $C_2H_2^+(X^2\Pi_u)$, which are shown in Table 3. Some of the reported spin−orbit coupling constants and rotational constants for the vibrational ground states are also listed in Table 3. It is seen that almost all the measurements are in agreements with each other within their experimental uncertainties. However, we provide presently the most accurate fundament frequency of ω_2 and also the first experimentally measured spin−orbit coupling constant and rotational constant for $v_2^+ = 1$.

D. Rotational Bands of $v_4^+ = 1$ and $v_5^+ = 1$ with $K = 0$. We have recorded five rotationally resolved vibronic bands with $K = 0$, i.e., $4_1^1(\kappa^2\Sigma_u^+)$ (hot band), $4_0^1(\mu/\kappa^2\Sigma_u^{-/+})$, and $5_0^1(\mu/\kappa^2\Sigma_g^{+/-})$. Figures 7−9 show the measured spectra and the corresponding assignments for them, respectively.

The hot band $4_1^1(\kappa^2\Sigma_u^+)$ has been observed in the PES spectra; however, even the band origins could not be determined definitely due to the weak signals and low spectral resolution.[6] Partially resolved rotational structures for $v_4^+ = 1$ vibronic band have been obtained by two-photon excitation ZEKE spectroscopic method by Pratt et al.[7] For $v_5^+ = 1$, only partially resolved vibrational structure has been determined by laser-induced reaction method.[8] Our spectra provide the first rotationally resolved vibrational bands for $K = 0$ state of $v_4^+ = 1$ and $v_5^+ = 1$.

As discussed in section IIB (see Figure 2), the vibronic bands of the transitions from the ground vibrational state to $K = 0$ state have fewer rotational lines than the vibronic bands to $K = 1$ state. However, for hot band $4_1^1(\kappa^2\Sigma_u^+)$, because the

TABLE 2: Line Positions and Assignments for the ZEKE Spectra of C_2H_2[a]

	ion				ion		
position		J^+	neutral J''	position		J^+	neutral J''
	$0_0^0(^2\Pi_u)$				$2_0^1(^2\Pi_u)$		
91921.8		F_1 11/2	7	93759.5		F_1 3/2	3
91923.5		F_1 5/2	5	93765.1		F_1 5/2	3
91939.4		F_1 3/2	3	93766.7		F_1 3/2	2
91940.6		F_1 9/2	5	93772.5		F_1 7/2	3
91961.8		F_1 9/2	3	93773.8		F_1 3/2	0
91944.8		F_2 9/2	7	93776.6		F_1 5/2	1
91957.0		F_2 5/2	5	93784.2		F_1 7/2	1
91980.9		F_2 1/2	1	93793.8		F_1 11/2	3
91984.4		F_2 3/2	1	93800.2		F_2 1/2	1
91986.3		F_2 7/2	3	93803.6		F_2 3/2	1
91987.8		F_2 11/2	5	93809.3		F_2 5/2	1
				93817.3		F_2 7/2	1
	$4_0^1(^2\Sigma_u)$				$5_0^1(^2\Sigma_g)$		
92441.1	μ	F_1 3/2	3	92636.0	μ	F_2 1/2	3
92445.9	μ	F_1 1/2	2	92641.4	μ	F_1 1/2	2
92452.9	μ	F_1 3/2	1	92648.5	μ	F_1 3/2	1
92459.7	μ	F_2 3/2	0	92654.2	μ	F_1 3/2	0
92464.0	μ	F_2 5/2	1	92655.7	μ	F_1 5/2	0
92855.8	κ	F_1 5/2	3	92658.1	μ	F_2 5/2	1
92861.0	κ	F_1 1/2	1	92695.2	κ	F_2 3/2	1
92867.7	κ	F_2 3/2	1	92696.8	κ	F_1 5/2	1
92871.5	κ	F_2 7/2	3	92699.4	κ	F_1 7/2	2
92876.7	κ	F_2 5/2	0	92710.4	κ	F_2 7/2	1
92883.3	κ	F_2 7/2	1				
92889.7	κ	F_2 9/2	2				
92895.9	κ	F_2 11/2	3				
	$4_0^2(^2\Pi_u)$				$4_1^1(^2\Sigma_u)$		
93037.8	μ	F_1 7/2	5	92249.4	κ	F_1 1/2	1
93059.4	μ	F_1 3/2	1	92251.6	κ	F_2 1/2	1
93064.0	μ	F_1 5/2	1	92256.1	κ	F_2 3/2	1
93067.7	μ	F_1 9/2	3	92262.7	κ	F_2 5/2	1
93080.3	μ	F_2 7/2	1				
93092.5	μ	F_2 11/2	3				
93635.6	κ	F_1 7/2	3		$4_0^1 5_0^1(^2\Pi_g)$		
93655.3	κ	F_1 11/2	3	93149.3	μ	F_2 1/2	3
93628.5	κ	F_2 3/2	3	93161.0	μ	F_2 1/2	1
93640.4	κ	F_2 3/2	1	93165.6	μ	F_1 5/2	1
93647.1	κ	F_2 5/2	1	93167.6	μ	F_2 3/2	0

[a] All units are in cm^{-1}. "F_1" ("F_2") represents the energy level of the same J^+ but with lower (higher) rotational energy. The relative uncertainties of line positions are ± 0.2 cm^{-1}. The absolute uncertainties are ± 1 cm^{-1}. The differences between the experimental line positions with the calculated ones using the spectroscopic constants in Table 4 are within 0.2 cm^{-1}.

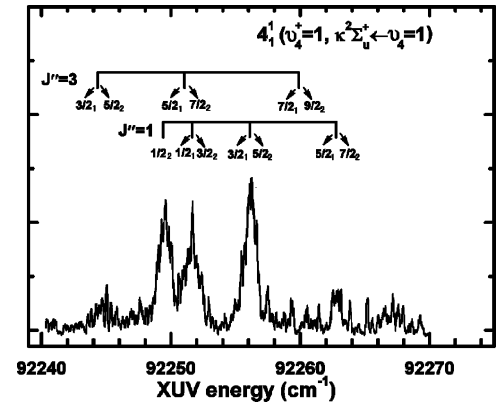

Figure 7. ZEKE spectrum and assignments for hot band $C_2H_2^+(\kappa^2\Sigma_u^+,\upsilon_4^+=1) \leftarrow C_2H_2(X^1\Sigma_g^+,\upsilon_4=1)$. The subscript 1 (2) in the figure means that the rotational energy level is F_1 (F_2).

lower state has $K = 1$, the nuclear symmetry selection rules do not change the outlook of the spectra and more lines will appear in comparison with the case of $K = 0$. This fact is demonstrated by comparing Figure 7 with Figures 8 and 9.

TABLE 3: Ionization Potential (IP) of C_2H_2, Spin−Orbit Coupling Constant A_v and Symmetric C≡C Stretching Fundamental Frequency ω_2 of $C_2H_2^+(X^2\Pi_u)$[a]

method	IP	$A_{so}(\upsilon_2^+=0)$	B_0^+	ω_2	ref
PIE[b]	91915(24)			1860(27)	22
PES[c]	91996(40)			1807(16)	23
PES[c]	91971(40)	32(8)		1817(25)	6
TPES[d]	91947(40)			1801(30)	24
PIE[e]	91956(1)				25
IR[f]		−30.91(2)	1.10463(2)		26
ZEKE[g]	91952(2)	−30		1803 ∼ 1828	7
ZEKE[g]	91953.5(5)	−30.86(44)	1.110(10)		9
ZEKE[g]	91953.5(10)	−30.77(30)	1.104(6)	1817.5(10)	this work

[a] All units are cm^{-1}. The digits in parentheses represent uncertainties in the last significant figures quoted. $\omega_2 = T_v(\upsilon_2^+=1) - T_v(\upsilon_2^+=0)$, where T_v can be found in Table 1. [b] Photoionization efficiency curve. [c] Photoelectron spectroscopy. [d] Threshold photoelectron spectroscopy. [e] (3+1) multiphoton ionization efficiency. [f] IR absorption method. [g] Zero kinetic energy photoelectron spectroscopy.

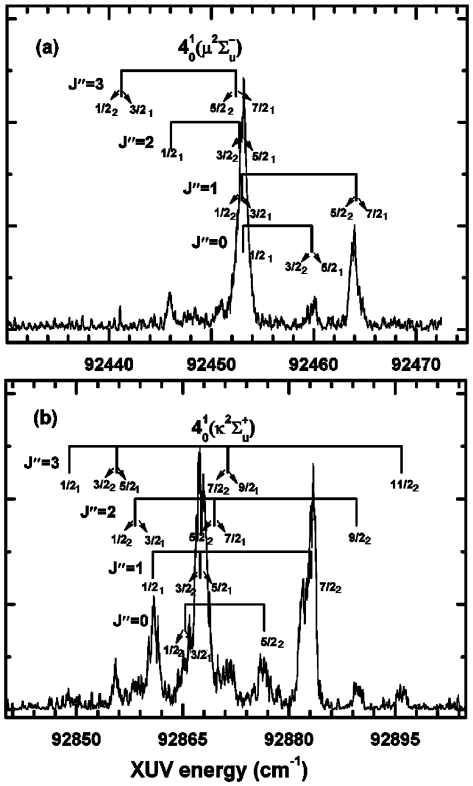

Figure 8. ZEKE spectra and assignments for (a) $C_2H_2^+(\mu^2\Sigma_u^-,\upsilon_4^+=1) \leftarrow C_2H_2(X^1\Sigma_g^+)$ and (b) $C_2H_2(\kappa^2\Sigma_u^+,\upsilon_4^+=1) \leftarrow C_2H_2(X^1\Sigma_g^+)$. The subscript 1 (2) in the figure means that the rotational energy level is F_1 (F_2).

For $K = 0$, the spin−orbit energy splitting will be decreased greatly in comparison with that of the ground vibrational state due to the zero projection of orbit angular momentum on the molecular axis.[11] The rotational energy levels can be described using Hund's case (b) and analytical formulas have been derived by Hougen using perturbation theory.[11] We used the formalism described in section IIIA to obtain the spectroscopic constants. All five rotational bands of $K = 0$ observed were used as a whole in the fitting process. The obtained spectroscopic constants are listed in Table 4 along with the results from $K = 1$ bands described in next section. The transition lines used in the fitting are listed Table 2.

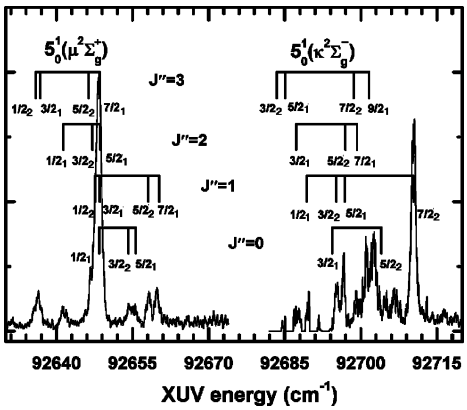

Figure 9. ZEKE spectrum and assignments for $C_2H_2^+(\mu^2\Sigma_g^+,v_5^+=1) \leftarrow C_2H_2(X^1\Sigma_g^+)$ and $C_2H_2^+(\kappa^2\Sigma_g^-,v_5^+=1) \leftarrow C_2H_2(X^1\Sigma_g^+)$. The subscript 1 (2) in the figure means that the rotational energy level is F_1 (F_2).

TABLE 4: Spectroscopic Constants Obtained in the Nonlinear Least Square Fitting of the Vibronic Bands[a]

	$v_4^+=1,v_5^+=1$ Σ^b	$v_4^+=2,v_5^+=2,v_4^+=v_5^+=1$ Π^c
A_{SO}	−31.42(22)	−31.50(26)
$B^+(0,0)$	[1.104]	[1.104]
$B^+(1,0)$	1.112(9)	[1.112]
$B^+(0,1)$	1.125(16)	[1.125]
$B^+(1,1)$	[1.08]	1.04(6)
$B^+(2,0)$	[1.10]	1.101(8)
$B^+(0,2)$	[1.10]	[1.10]
$B^+(i,j)$	[1.08]	[1.08]
ω_4	692.32(12)	696.27(6)
ϵ_4	0.2923(2)	0.2901(2)
ω_5	704.05(13)	706.68(17)
ϵ_5	0.0219(3)	0.019(3)

[a] Equations 10−12 were used to calculate the rovibronic energy levels. The Renner−Teller parameters have no units and all other parameters have units of cm^{-1}. The numbers in "( )" represent uncertainties in the last significant figures quoted. The numbers in "[ ]" were fixed and not optimized in the fitting processes. The $B^+(i,j,)$ represents all rotational constants other than those listed in the table. [b] Five rotationally resolved vibronic bands of $4_1^1(\kappa^2\Sigma_u^+)$ (hot band), $4_0^1(\mu/\kappa^2\Sigma_u^{-/+})$, $5_0^1(\mu/\kappa^2\Sigma_g^{+/-})$ have been used in the fitting. [c] Three rotationally resolved vibronic bands of $4_0^2(\mu^2\Pi_u)$, $4_0^15_0^1(\mu^2\Pi_g)$, and $4_0^2(\mu^2\Pi_u)$ have been used in the fitting.

It should be noted that only the rotationally resolved spectra can be used to determine the sign of Renner−Teller parameters ϵ. Our results show that the measured spectra can be assigned properly only when ϵ_4 and ϵ_5 are positive. For ϵ_5, this is the first definite experimental result which confirm the most recent theoretical studies.[12,14]

E. Vibronic Bands of $v_4^+=2$, $v_5^+=2$, and $v_4^+=v_5^+=1$ with $K=1$. We have recorded five rotationally resolved vibronic bands with $K=1$, i.e., $4_0^2(\mu^2\Pi_u)$, $4_0^2(\kappa^2\Pi_u)$, $4_0^15_0^1(\mu^2\Pi_g)$, $0_0^0(X^2\Pi_u)$, and $2_0^1(X^2\Pi_u)$. The last two vibrational bands are shown in Figure 6a,b and have been discussed in section IIIC. Figures 10 and 11 show the measured spectra for the first two vibronic bands, the third vibronic bands and the corresponding assignments for them, respectively.

We used the formalism described in section IIIA to obtain the spectroscopic constants. Three vibronic bands were used in the fitting process, i.e, $4_0^2(\mu^2\Pi_u)$, $4_0^15_0^1(\mu^2\Pi_g)$, and $4_0^2(\kappa^2\Pi_u)$. The obtained spectroscopic constants are listed in Table 4. The lines used in the fitting are listed Table 2. From Table 4, it is seen that there are some differences between the constants obtained from using vibronic bands of $v_4^+=1$ and $v_5^+=1$ with $K=0$ and $v_4^+=2$, $v_5^+=2$, and $v_4^+=v_5^+=1$ with $K=1$. This may arise from anharmonicities of the vibrations. Because only the first overtones and first combination bands were observed for the bending excitation, we have not introduced the anharmonicity constants in the fitting.

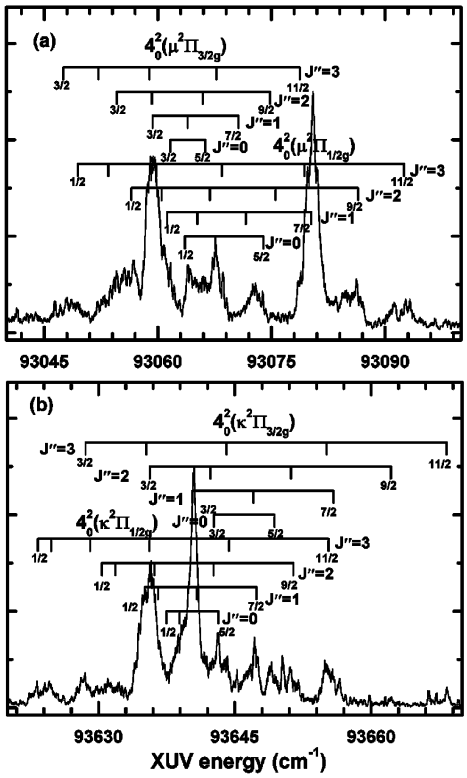

Figure 10. ZEKE spectra and assignments for (a) $C_2H_2^+(\mu^2\Pi_u,v_4^+=2) \leftarrow C_2H_2(X^1\Sigma_g^+)$ and (b) $C_2H_2^+(\kappa^2\Pi_u,v_4^+=2) \leftarrow C_2H_2(X^1\Sigma_g^+)$.

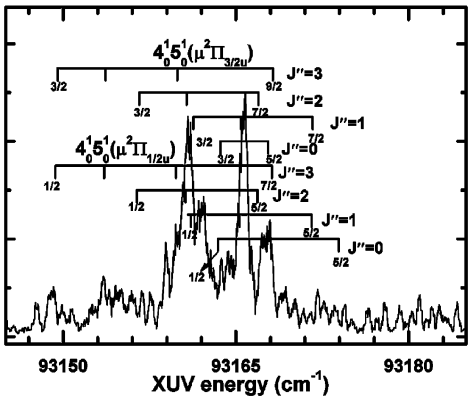

Figure 11. ZEKE spectrum and assignments for $C_2H_2^+(\mu^2\Pi_g,v_4^+=1,v_5^+=1) \leftarrow C_2H_2(X^1\Sigma_g^+)$.

As shown in Figure 4, there are totally seven vibronic bands of $K=1$ due to the coupling of the vibrational angular momentum with electronic orbital angular momentum. We observed and assigned three of the seven vibronic bands. In the order of increasing energy, the seven bands are $4_0^2(\mu^2\Pi_u)$, $4_0^15_0^1(\mu^2\Pi_g)$, $5_0^2(\mu^2\Pi_u)$, $4_0^15_0^1(U^2\Pi_g)$, $4_0^15_0^1(\kappa^2\Pi_g)$, and $4_0^2(\kappa^2\Pi_u)$. The $4_0^15_0^1(U^2\Pi_g)$ vibronic state is the so-called unique state and its spin−orbit energy splitting should be similar to that of the ground vibrational state of the ion. For all other states, the spin−orbit energy splittings will be quenched due to the Renner−Teller interaction.

Pratt and co-workers have obtained partially rotationally resolved vibronic bands of $4_0^2(\mu^2\Pi_u)$.[7] In their spectra, a vibronic band around 93 160 cm^{-1} was not assigned definitely.

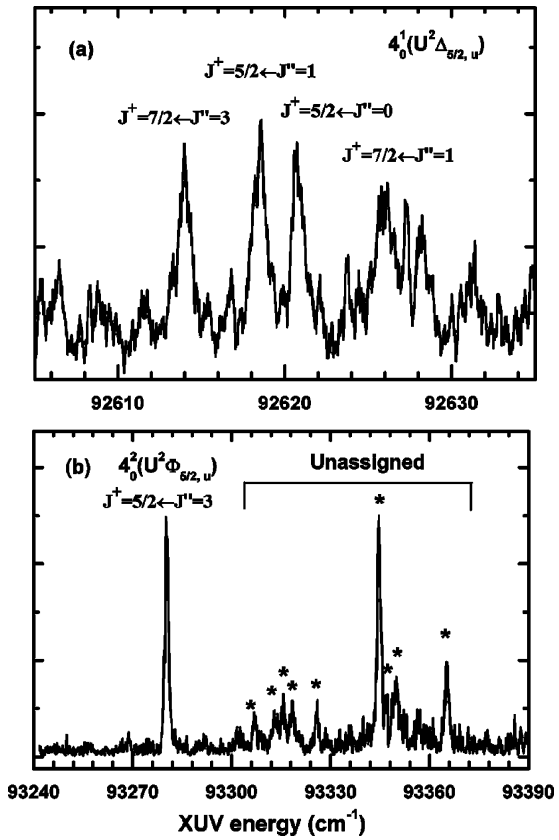

Figure 12. ZEKE spectra and assignments for transition to (a) $4_0^1(U^2\Delta_{5/2u})$, and (b) $4_0^2(U^2\Phi_{5/2u})$. The symbols * in (b) represent unassigned line positions listed in Appendix.

TABLE 5: Comparison of the Spectroscopic Constants[a]

method	ω_4	ϵ_4	ω_5	ϵ_5	ref
LIR[b]			710(4)	0.035	8
two-photon ZEKE[c]	694	0.30			7
theoretical[d]	704.48	0.3065	724.19	0.0130	14
ZEKE[e]	692.32(12)	0.2923(2)	704.05(13)	0.0219(3)	this work
ZEKE[f]	696.27(6)	0.2901(2)	704.05(13)	0.019(3)	this work

[a] The bending frequencies ω_4 and ω_5 are in cm^{-1} and Renner−Teller parameters ϵ_4 and ϵ_5 have no units. [b] By laser-induced reaction, the upper limit for ϵ_5 was reported as 0.037. [c] By ZEKE spectroscopy with two-color double resonance excitation using $\tilde{A}^1A_u$ as the intermediate state. The uncertainties of the parameters have not been reported. [d] Theoretical calculations. [e] ZEKE spectroscopy with one photon excitation by fitting the vibronic bands $4_1^1(\kappa^2\Sigma_u^+)$ (hot band), $4_0^1(\mu/\kappa^2\Sigma_u^{-/+})$, and $5_0^1(\mu/\kappa^2\Sigma_g^{+/-})$. [f] ZEKE spectroscopy with one photon excitation by fitting the vibronic bands $4_0^2(\mu^2\Pi_u)$, $4_0^15_0^1(\mu^2\Pi_g)$, and $4_0^2(\kappa^2\Pi_u)$.

From our results, the spectra they observed should be assigned as $4_0^15_0^1(\mu^2\Pi_g)$. This vibronic band is related to simultaneous excitation of two bending modes and has not been observed before this work. However, we have not observed the vibronic band $4_0^15_0^1(\kappa^2\Pi_g)$. The reason for this is not clear to us. The $4_0^15_0^1(U^2\Pi_g)$ band may overlap with its neighbor band (see Figure 4) and is difficult to assign.

F. Other Vibronic Bands. For photon energies around 92 615 cm^{-1}, very weak signals have been observed as shown in Figure 12a. Using the predicted line positions calculated from the parameters listed in Table 4, they are assigned to be from the vibronic band $4_0^1(U^2\Delta_{5/2u})$. Four lines have been assigned tentatively and are listed in Table 6. The measured data have shifts about 1.4 cm^{-1} relative to the predicted line positions.

TABLE 6: Line Positions[a] and Tentative Assignments[b] for Vibronic Bands $4_0^1(U^2\Delta_u)$ and $4_0^2(U^2\Phi_u)$

upper state		lower state		
		J^+	J''	exp − cal
		$4_0^1(U^2\Delta_u)$[b]		
92614.1	F_1	7/2	3	1.4
92618.5	F_1	5/2	1	1.5
92620.8	F_1	5/2	0	1.5
92625.9	F_1	7/2	1	1.4
		$4_0^2(U^2\Phi_u)$[b]		
93280.3	F_2	5/2	3	−1.7

[a] The relative uncertainties of line positions are ±0.2 cm^{-1}. The absolute uncertainties are ±1 cm^{-1}. [b] The calculations used the spectroscopic constants listed in Table 4.

TABLE 7: Calculated Lowest Rotational Energy Levels for the Vibronic States of $C_2H_2^+(X^2\Pi_u)$ Due to the Renner−Teller Effect[a]

vibration	vibronic state	level	vibration	vibronic state	level
$v^+=0$	$^2\Pi_{3/2u}$	0			
	$^2\Pi_{1/2u}$	29.8			
$v_4^+=1$	$\mu^2\Sigma_u^-F_1$	499.5	$v_5^+=1$	$\mu^2\Sigma_g^+F_1$	694.9
	$\mu^2\Sigma_u^-F_2$	501.7		$\mu^2\Sigma_g^+F_2$	696.5
	$U^2\Delta_{5/2u}$	672.9		$U^2\Delta_{5/2g}$	713.4
	$U^2\Delta_{3/2u}$	701.4		$U^2\Delta_{3/2g}$	743.0
	$\kappa^2\Sigma_u^+F_1$	909.9		$\kappa^2\Sigma_g^-F_1$	738.2
	$\kappa^2\Sigma_u^+F_2$	912.1		$\kappa^2\Sigma_g^-F_2$	739.8
$v_4^+=2$	$\mu^2\Pi_{3/2u}$	1108.3	$v_5^+=2$	$\mu^2\Pi_{3/2u}$	1404.8
	$\mu^2\Pi_{1/2u}$	1110.0		$\mu^2\Pi_{1/2u}$	1399.9
	$U^2\Phi_{7/2u}$	1316.0		$U^2\Phi_{7/2u}$	1410.7
	$U^2\Phi_{5/2u}$	1342.7		$U^2\Phi_{5/2u}$	1440.5
	$\kappa^2\Pi_{1/2u}$	1683.5		$\kappa^2\Pi_{1/2u}$	1451.2
	$\kappa^2\Pi_{3/2u}$	1685.3		$\kappa^2\Pi_{3/2u}$	1449.3
$v_4^+=v_5^+=1$	$\mu^2\Pi_{3/2g}$	1210.2			
	$\mu^2\Pi_{1/2g}$	1209.9			
	$U^2\Phi_{7/2g}$	1370.4			
	$U^2\Phi_{5/2g}$	1398.9			
	$U^2\Pi_{3/2g}$	1373.1			
	$U^2\Pi_{1/2g}$	1401.6			
	$\kappa^2\Pi_{1/2g}$	1620.6			
	$\kappa^2\Pi_{3/2g}$	1620.4			

[a] The spectroscopic constants used in the calculation are listed in Table 4. All units are in cm^{-1}.

Pratt and co-workers have observed $4_0^1(U^2\Delta_u)$ band with unresolved rotational structure.[7] The rovibronic line positions of $4_0^1(U^2\Delta_{5/2u})$ assigned by us are in the range of those reported by Pratt and co-workers.

One strong peak has been found at 93 280.3 cm^{-1} as shown in Figure 12b. This peak is the real ZEKE signal and is not from the autoionization of C_2H_2. The calculation using the parameters in Table 4 showed that this line may be assigned tentatively as ($v_4^+=2$, $U^2\Phi_{5/2u}$, $J^+=2.5$) ← ($X^1\Sigma_g^+$, $v''=0$, $J''=3$). This assignment is consistent with a tentative assignment by Pratt and co-workers who observed a very weak vibronic band in this region.[7]

Some of the rotational lines in Figure 12b are difficult to be assign because several vibronic bands are expected to appear in this energy range such as $4_0^15_0^1(U^2\Pi_g)$, $4_0^15_0^1(U^2\Phi_g)$, $5_0^2(\mu^2\Pi_u)$, and $5_0^2(U^2\Phi_u)$. The unassigned line positions are listed in Appendix. More detail experiments are needed to obtain definite assignments for them.

G. Renner−Teller Vibronic Energy Structure. The Renner−Teller parameters for the two bending modes of $C_2H_2^+$-($X^2\Pi_u$) have been reported previously and are listed in Table 5

along with our results. The Renner−Teller parameters for the trans bending vibration by Pratt and co-workers were obtained by partially resolved rotational bands.[7] The Renner−Teller parameters for the cis bending vibration were obtained by partially resolved vibrational bands.[8] The parameters obtained by us using several fully rotationally resolved vibronic bands are consistent with those of the earlier results but with much higher accuracy.

Using the Renner−Teller parameters and other spectroscopic constants listed in Table 4, we have calculated the lowest energy levels of all vibronic states for energies about 2000 cm^{-1} above the ground vibrational state of $C_2H_2^+(X^2\Pi_u)$. The results are shown in Table 7 and also in Figure 4. Thus, we have a glimpse of the rovibronic energy structure up to 2000 cm^{-1} for this simplest tetratomic linear molecular ion.

V. Conclusions

We obtained the rotationally resolved ZEKE spectra of C_2H_2 using XUV laser. The vibronic bands up to 2000 cm^{-1} above the ground vibrational state of $C_2H_2^+(X^2\Pi_u)$ have been recorded. The assigned vibronic bands are $4_1^1(\kappa^2\Sigma_u^+)$ (hot band), $4_0^1(\mu/\kappa^2\Sigma_u^{-/+})$, $5_0^1(\mu/\kappa^2\Sigma_g^{+/-})$ and also $4_0^2(\mu^2\Pi_u)$, $4_0^2(\kappa^2\Pi_u)$, $4_0^1 5_0^1(\mu^2\Pi_g)$, $0_0^0(X^2\Pi_u)$, and $2_0^1(X^2\Pi_u)$, where 2_0^n, 4_0^n, and 5_0^n represent the symmetric C≡C stretching, the CCH trans and cis bending vibrational excitations, respectively.

To obtain the Renner−Teller parameters from the rotationally resolved vibrational bands, the previous treatments for triatomic molecules usually replace the off-diagonal Renner−Teller terms by diagonal energy corrections. Instead of this method, we set up a Hamiltonian that considers simultaneously the Renner−Teller coupling, vibrational energies, rotational energies, and spin−orbit coupling interaction. By fitting the observed spectra with the eigenvalues from this Hamiltonian, we obtained the Renner−Teller parameters, the harmonic frequencies, the spin−orbit coupling constants, and the rotational constants associated with the vibronic bands.

Acknowledgment. We acknowledge the research supports by the National Science Foundation of China under Project Nos. 20273038 and 10274041 and the Scientific Research Program of Tsinghua University.

Appendix A

The unassigned line positions in panel b of Figure 12. Units are in cm^{-1}. The absolute uncertainties are ± 1 cm^{-1} and the relative uncertainties are ± 0.2 cm^{-1}.

unassigned lines
93307.0
93313.0
93315.5
93318.3
93325.9
93344.7
93346.8
93349.8
93365.2

References and Notes

(1) Herzberg, G. *Molecular spectra molecular structure, III electronic spectra electronic structure of polyatomic molecules*; D Van Nostrand Co., Inc.: Princeton, NJ, 1966.
(2) Brown, J. M. *Computational Molecular Spectroscopy*; Jensen, P., Ed.; Bunker Wiley P. R.: New York, 2000; p 517.
(3) Tang, J.; Saito, S. *J. Chem. Phys.* **1996**, *105*, 8020.
(4) He, S. G.; Clouthier, D. J. *J. Chem. Phys.* **2005**, *123*, 014316.
(5) He, S. G.; Clouthier, D. J. *J. Chem. Phys.* **2005**, *123*, 014317.
(6) Reutt, J. E.; Wang, L. S.; Pollard, J. E.; Trevor, D. J.; Lee, Y. T.; Shirley, D. A. *J. Chem. Phys.* **1986**, *84*, 3022.
(7) Pratt, S. T.; Dehmer, P. M.; Dehmer, J. L. *J. Chem. Phys.* **1993**, *99*, 6233.
(8) (a) Asvany, O.; Giesen, T.; Redlich, B.; Schlemmer, S. *Phys. Rev. Lett.* **2005**, *94*, 073001. (b) Schlemmer, S.; Asvany, O.; Giesen, T. *Phys. Chem. Chem. Phys.* **2005**, *7*, 1592.
(9) Rupper, P.; Merkt, F. *Rev. Sci. Instrum.* **2004**, *75*, 613.
(10) Pople, J. A. *Mol. Phys.* **1960**, *3*, 16.
(11) Hougen, J. T. *J. Chem. Phys.* **1962**, *36*, 519.
(12) Peric, M.; Thummel, H.; Marian, C. M.; Payerimhoff, S. D. *J. Chem. Phys.* **1995**, *102*, 7142.
(13) Peric, M.; Ostojic, B.; Engels, B. *J. Chem. Phys.* **1998**, *109*, 3086.
(14) Peric, M.; Payerimhoff, S. D. *J. Mol. Spectrosc.* **2002**, *212*, 142.
(15) Mo, Y.; Yang, J.; Chen, G. *J. Chem. Phys.* **2004**, *120*, 1263.
(16) Li, M.; Coxon, J. A. *J. Chem. Phys.* **1995**, *102*, 2663.
(17) Brown, J. M. *Mol. Phys.* **2003**, *101*, 3419.
(18) Yang, D. S.; Zgierski, M. Z.; Rayner, D. M.; Hackett, P. A.; Martinez, A.; Salahub, D. R.; Roy, P.-N.; Carrington, T., Jr. *J. Chem. Phys.* **1995**, *103*, 5335.
(19) Berces, A.; Zgierski, M. Z.; Yang, D. S. In *Computational Molecular Spectroscopy*; Jensen, P., Bunker, P., Eds.; Wiley: New York, 2000.
(20) Yang, J.; Mo, Y.; Lau, K. C.; Song, Y.; Qian, X. M.; Ng, C. Y. *Phys. Chem. Chem. Phys.* **2005**, *7*, 1518.
(21) Zare, R. N. *Angular Momentum*; Wiley: New York, 1998.
(22) Ono, Y.; Osuch, E. A.; Ng, C. Y. *J. Chem. Phys.* **1982**, *76*, 3905.
(23) Dehmer, P. M.; Dehmer, J. L. *J. Electron Spectrosc. Relat. Phenom.* **1982**, *28*, 145.
(24) Avaldi, L.; Dawber, G.; Hall, R. I.; King, G. C.; McConkey, A. G.; MacDonald, M. A.; Stefani, G. *J. Electron Spectrosc. Relat. Phenom.* **1995**, *71*, 93.
(25) Shafizadeh, N.; Fillion, J.-H.; Gauyacq, D.; Couris, S. *Philos. Trans. R. Soc. London A* **1997**, *355*, 1637.
(26) Jagod, M.-F.; Rosslein, M.; Gabrys, C. M.; Rehfuss, B. D.; Scappini, F.; Crofton, M. W.; Oka, T. *J. Chem. Phys.* **1992**, *97*, 7111.
(27) Watson, J. K. G.; Herman, M.; Van Craen, J. C.; Colin, R. *J. Mol. Spectrosc.* **1982**, *95*, 101.